Brain Structure and Function (2020) 225:621–638
https://doi.org/10.1007/s00429-020-02025-6

ORIGINAL ARTICLE

Dense projection of Stilling's nucleus spinocerebellar axons that convey tail proprioception to the midline area in lobule VIII of the mouse cerebellum

Yuanjun Luo[1] · Takeru Onozato[1] · Xuanjing Wu[1] · Kazuma Sasamura[1] · Kenji Sakimura[3] · Izumi Sugihara[1,2]

Received: 28 March 2019 / Accepted: 7 January 2020 / Published online: 18 January 2020

Abstract

The cerebellar cortex has dual somatotopic representation, broadly in the anterior lobules and narrowly in the posterior lobules. However, the somatotopy has not been well understood in vermal lobule VIII, located in the center of the posterior representation. Here, we examined the axonal projections and somatosensory representation of the midline area of vermal lobule VIII in mice, using the striped zebrin expression pattern as a landmark of intra-lobular compartmentalization. Retrograde tracer injection into this area (zebrin stripes 1+ and 1− in lobule VIII) labeled neuronal clusters, bilaterally, in the pericanal gray matter (Stilling's nucleus) in the sacral spinal cord. Spinocerebellar axons labeled by biotinylated dextran amine injection into the sacral pericanal gray matter terminated bilaterally in stripes 1+ and 1− in lobule VIII, with more than 70 terminals per axon, and the vermal stripes in lobules II–III. Dorsal flexion of the tail and electrical stimulation of the sacral spinal gray matter elicited the firing of mossy fiber terminals in stripes 1+ and 1− in lobule VIII. Anterograde labeling of Purkinje cell axons in this area showed terminals in the medial pole of the medial cerebellar nucleus. Lesioning of this area impaired locomotor performance in the rotarod test. These results demonstrated that stripes 1+ and 1− in lobule VIII receive tail proprioceptive sensation from the Stilling's nucleus as their predominant mossy fiber input. The results also suggest that locomotion-related activity is represented not only in the anterior lobule, but also in lobule VIII in the cerebellar vermis.

Keywords Cerebellar mossy fibers · Aldolase C · Cerebellar cortex · Cerebellar nucleus · Spinal cord · Locomotion

Introduction

The cerebellar cortex is subdivided transversely by its lobular folding (Larsell 1952) and longitudinally by compartments of Purkinje cell (PC) subsets that are defined by the expression pattern of certain molecules, including aldolase C or zebrin (Brochu et al. 1990; Voogd and Ruigrok 1997). Longitudinal stripes in each lobule have specific topographic projection patterns of efferent PC axons and afferent olivocerebellar axons (Voogd et al. 2003; Sugihara and Shinoda 2004; Sugihara et al. 2009). Mossy fiber projection patterns are also related to both lobular structures and longitudinal stripes (Quy et al. 2011; Luo et al. 2018; Pijpers et al. 2006). Through these different projection patterns, each subarea of the cerebellar cortex defined by the stripe and lobule is supposedly involved in a particular function (Ruigrok 2011; Horn et al. 2010).

The somatosensorimotor function related to a specific body part, or somatotopy, has dual representation in the cerebellar cortex, broadly in the anterior lobules (lobules I–VIa) and narrowly in the posterior lobules (lobules VIII and IXa–b, and parts of hemispheric lobule VII) whereas the cognitive, oculomotor and visuomotor functions are represented in the central lobules (lobules VIb–c and VII) (Stoodley et al. 2012). In the anterior lobules, the vermal part is involved in

Yuanjun Luo and Takeru Onozato contributed equally.

✉ Izumi Sugihara
isugihara.phy1@tmd.ac.jp

[1] Department of Systems Neurophysiology, Graduate School of Medical and Dental Sciences, Tokyo Medical and Dental University, 1-5-45 Yushima, Bunkyo-ku, Tokyo 113-8519, Japan

[2] Center for Brain Integration Research, Tokyo Medical and Dental University, 1-5-45 Yushima, Bunkyo-ku, Tokyo 113-8519, Japan

[3] Department of Animal Model Development, Brain Research Institute, Niigata University, 1-757 Asahimachi, Niigata 951-8585, Japan

gross somatosensorimotor function such as locomotion and antigravity posture maintenance (Muzzu et al. 2018), while the paravermal and hemispheric parts are involved in finer somatosensorimotor function of specific body parts such as the limbs (Ekerot et al. 1987) and eyelids (Mostofi et al. 2010). In the posterior lobules, the paravermal and hemispheric areas are also involved in the control of the sensorimotor activity of specific parts of the limbs and head (Atkins and Apps 1997; Cerminara et al. 2013; Welker 1987). However, the somatotopy in vermal lobule VIII has not been well clarified.

To determine the functional localization of the cerebellar cortical areas, axonal connectivity and sensory responsiveness are essential. Vermal lobule VIII contains clearly delineated similarly wide zebrin-positive (Z+) and zebrin-negative (Z−) stripes (Fujita et al. 2014; Nguyen-Minh et al. 2019), which can facilitate the analysis of axonal projection patterns. Climbing fiber and Purkinje cell projections are distinctively arranged according to zebrin stripes. The general topographic scheme of these projections (Sugihara and Shinoda 2004; Sugihara et al. 2009) suggests that climbing fiber axons originating from several areas in the caudal part of the medial accessory olive project to zebrin stripes in lobule VIII, and Purkinje cells in Z+ and Z− stripes project to the caudoventral and rostrodorsal parts of the medial cerebellar nucleus although the specific topographic connections to and from lobule VIII zebrin stripes have yet to be determined. Moreover, the main mossy fiber input to lobule VIII has not been fully demonstrated. Spinocerebellar and cuneocerebellar mossy fiber axons project to both the anterior and posterior lobules by branching, thus, providing some branches to vermal lobule VIII (Quy et al. 2011; Luo et al. 2018; Matsushita and Ikeda 1980). Specifically, spinocerebellar neurons in the Stilling's nucleus in the pericanal gray matter of the sacral spinal cord (Edgley and Grant 1991) and those in the lower thoracic and lumbar spinal cord (Reeber et al. 2011; Sengul et al. 2015) may be the major sources of mossy fiber projections to lobule VIII.

In this study, our aims were to identify the projections of mossy fibers and Purkinje cell axons, and to examine the functional significance of the midline area (zebrin stripes 1+ and 1−) in vermal lobule VIII in the mouse. For this purpose, we performed anterograde and retrograde tracing of axons, electrophysiological recordings from the cerebellar cortex and behavioral observation in lesioned mice. Zebrin (aldolase C) stripes were visualized with immunostaining or with genetic manipulation (Aldoc-Venus mice Fujita et al. 2014) in these experiments.

Materials and methods

Ethics statements

Experimental protocols were approved by the Animal Care and Use Committee (A2018-147C, A2018-260C, A2018-222C, A2017-063A, A2017-062A, 017097A) and Gene Recombination Experiment Safety Committee (2012-064C4, 2017-040A) of Tokyo Medical and Dental University.

Animals

Adult female wild-type mice of B6C3F1 background were used in anterograde labeling experiments and electrophysiology experiments with sacral spinal cord stimulation. The Aldoc-Venus knock-in mouse line of C57BL/6N background, which carries a transgene encoding a mutated fluorescent protein placed behind the translational initiation site of the Aldoc gene (Fujita et al. 2014, MGI:5620954), were used in all other experiments except for anterograde tracing of spinocerebellar axons. Aldoc-Venus knock-in mice were maintained by mating homozygotes. Heterozygotes were produced by mating Aldoc-Venus homozygous males with C57BL/6N females. Adult male and female heterozygotes (11–29 weeks old, 24–30 g) were used in retrograde labeling, response mapping and lesioning experiments. Female homozygotes, heterozygotes and wild type individuals obtained by mating heterozygotes were used in behavior experiments involving Aldoc-Venus mice.

Anterograde labeling of spinocerebellar axons from the sacral spinal cord

Adult male and female wild-type mice of B6C3F1 background were used. Mice were anesthetized by an intraperitoneal injection of ketamine (0.150 mg/g body weight) and xylazine (0.006 mg/g). Supplemental doses of ketamine (0.075 mg/g) and xylazine (0.003 mg/g) were given at 40 min interval, 1 h after the initial dose, as required. Alternatively, they were anesthetized by an intraperitoneal injection of a cocktail of medetomidine hydrochloride (0.75 µg/g body weight), midazolam (4.0 µg/g) and butorphanol tartrate (5.0 µg/g). No supplemental doses were required for up to 2 h, by which time our surgical procedures were completed. Atipamezole hydrochloride (0.75 µg/g body weight) was given intraperitoneally at the end of the surgical procedures.

Mice were placed in a stereotaxic apparatus in prone position with the head flat, on a platform with a heating pad (37 °C) to allow touch and various movements of the extremities and tail. An incision was made through the skin at the midline at the lower lumbar levels of the spine

(40–45 mm caudal to the skull). Laminectomy was made in the spine at the place 42 mm caudal to the caudal end of the skull and 10 mm caudal to the top position of the dorsal bend of the lumbar spinal columns (presumably L2 spine), after fixing the neighboring spine to the apparatus, to expose the sacral spinal cord. This surgery point was determined by referring to the dissected preparation (Luo et al. 2018) and magnetic resonance image (Harrison et al. 2013) of the spinal cord. A glass microelectrode (tip diameter, 10 µm) filled with biotinylated dextran amine (BDA) solution in saline (10%, BDA; D-7135, molecular weight 3000; Molecular Probes, Eugene, OR, USA) was inserted into the spinal cord (0.3 mm lateral, 0.5 mm deep). A pneumatic pressure pulse was applied using an electronic valve device (Picopump PV820, WPI, Sarasota, FL, USA) connected to a nitrogen tank to eject a drop of BDA solution (about 100 nl) from the pipette. The micropipette was withdrawn a few minutes after the injection, and the skin was sutured.

After a survival period of 21 days, the mice were anesthetized with an intraperitoneal injection of an overdose of pentobarbital (Abbott lab, Chicago, USA, 0.1 mg/g) and xylazine (0.005 mg/g). They were then perfused intracardially with phosphate-buffered saline (PBS) followed by a fixative containing 4% paraformaldehyde, NaCl 0.9%, phosphate buffer 10 mM (pH 7.4). While dissecting the spinal cord, the positions of the first and last ribs were marked on the surface with Alcian blue. Histological procedures for visualizing BDA and aldolase C in the dissected brain and spinal cords were the same as described previously (Luo et al. 2018). Briefly, serial coronal sections (80 µm thick) of the entire cerebellum and medulla, and serial sagittal sections (80 µm thick) of the entire spinal cord were processed with biotinylated peroxidase–avidin complex (PK6100 Elite ABC kit; Vector Laboratories, Burlingame, CA, USA) to visualize BDA in black. Then, serial coronal sections containing the cerebellum were processed with a biotin-conjugated anti-aldolase C antibody (320 ng/ml, #69076, Sugihara and Shinoda 2004; RRID: AB_2313920) to visualize aldolase C (zebrin) in brown. The sections were mounted on glass slides, dried, counterstained faintly with thionine, and coverslipped.

The methods of reconstruction of individual axons have been described before (Luo et al. 2018; Quy et al. 2011). Briefly, axonal trajectories were reconstructed manually from serial sections using a conventional bright-field microscope (BX50; Olympus, Tokyo, Japan) with a three-dimensional imaging attachment (Edge Spectra; SNT Microscopes LLC., Los Angeles, CA, USA) equipped with a camera lucida apparatus with objectives of 10×, 20×, 40×, 60× and 100×. Drawings of the axonal segment in serial sections were assembled using two-dimensional graphics software (Illustrator, Adobe, San Jose, CA, USA). The methods for mapping mossy fiber terminals on the unfolded cerebellar cortex have also been described before (Luo et al. 2018; Quy et al. 2011). Briefly, the location of a terminal was identified in relation to the immunostained aldolase C stripes on the section, and mapped upon the standardized unfolded representation of the Purkinje cell layer of the whole cerebellar cortex with the aldolase C labeling pattern (Sarpong et al. 2018). The methods for locating and mapping BDA injection sites in the spinal cord have been described (Luo et al. 2018).

Retrograde labeling of spinocerebellar neurons

Seven adult male and female heterozygous Aldoc-Venus:C57BL/6N mice (Fujita et al. 2014) were used in retrograde labeling experiments. Methods of retrograde labeling of spinocerebellar neurons and their mapping have been described previously (Luo et al. 2018). Mice were anesthetized in the same way as in the anterograde labeling experiments (above) and were placed in a stereotaxic apparatus in prone position with the head rotated by 60° nose down to open the skull above lobule VIII. Stripes were identified under a fluorescent macrozoom microscope (Olympus, VMX10), and a small cut was made in the dura above the target stripe in lobule VIII. A glass microelectrode (tip diameter, 20 µm) filled with latex bead suspension (Red beads, Lumafluor Inc., Durham, NC, USA) was inserted into the cerebellum (0.5 mm deep). A pneumatic pressure pulse was applied using the electronic valve device to eject a drop of suspension (about 20 nl) from the pipette. After a survival period of 14 days, the mice were anesthetized by intraperitoneal injection of an overdose of pentobarbital, and perfusion-fixed as above to dissect the cerebellum, medulla and spinal cord. While dissecting the spinal cord, the positions of the first and last ribs were marked on the surface with Alcian blue. Serial, frozen sections (80 µm thick, coronal sections for the brain, sagittal sections for the spinal cord) were cut and mounted on slides. They were coverslipped temporarily with PBS for observation and imaging. Methods for locating and mapping retrogradely labeled neurons in the spinal cord have been described (Luo et al. 2018). By comparing the positions of marks of the first and last ribs and the curvature of the whole spinal cord with those of our standard mouse spinal cord specimen (Fig. 1 of Luo et al. 2018), spinal segments were defined in sagittal sections. The position of labeled neurons was mapped in the drawing made with Illustrator from the digital image, if their nucleus was contained inside the section. Subsequently, the drawings of retrogradely labeled neurons, surface of the spinal cord, boundaries between the white and gray matters, and the central canal were imported into the three-dimensional software (Rhinoceros 4, Robert McNeel & Associates, Seattle, WA, USA). To re-map labeled neurons on a coronal plane, coronal trajectories of these elements were matched

with the drawing of the standard coronal spinal cord section at various segments prepared previously (Luo et al. 2018).

Anterograde labeling of Purkinje cell axons

Five adult male and female heterozygous Aldoc-Venus: C57BL/6N mice (Fujita et al. 2014) were used in anterograde labeling experiments. Methods of anterograde labeling and mapping of Purkinje cell axonal terminals have been described previously (Sarpong et al. 2018). Mice were anesthetized, placed and approached in the same way as other labeling experiments (above). After stripes were identified, a small cut was made in the dura above the target stripe in lobule VIII. A glass microelectrode (tip diameter, 5 µm) filled with dextran Alexa Fluor 594 dissolved in saline (10%; D-22913, molecular weight 10,000; Molecular Probes) was inserted into the cerebellum (0.15 mm deep). A pneumatic pressure pulse was applied using the electronic valve device to eject a drop of suspension (about 10 nl) from the pipette. After a survival period of 4 days, the mice were perfuse-fixed as above to dissect the cerebellum and medulla. Serial coronal sections (80 µm thick) were cut, mounted, observed and imaged as above. Methods for locating and mapping anterogradely labeled Purkinje cell terminals have been described (Sarpong et al. 2018). Briefly, the positions of the rostral pole of the anterior interposed nucleus and the caudal pole of the posterior interposed nucleus were defined as 100% and 0%, respectively, in the rostrocaudal axis. The relative position in percentile of sections containing labeled neuronal elements, which were imaged with the fluorescent microscope (below), was calculated. The three-dimensional model of the mouse cerebellar nuclei (Sarpong et al. 2018) was opened using Rhinoceros. The image of the coronal section was superimposed on it using a free software that makes its interface partially transparent (Extra Buttons, extrabuttons.com). Then, the location of the labeled neuronal components was demarcated using the "curve" command in Rhinoceros. Finally, the "loft" command of Rhinoceros was used to form a three-dimensional solid object to represent the distribution of the labeled neuronal components in the three-dimensional scheme of the CN.

Acquisition of digital images

Whole-mount specimens (fluorescent or bright field) were imaged using a cooled color CCD camera (DP-70, Olympus, Tokyo, Japan) attached to a macrozoom microscope (MVX10, Olympus). Low magnification images of serial sagittal sections of spinal cord samples of both the anterograde and retrograde labeling experiments were digitized using a digital scanner (Dimage AF-5000, Minolta, Osaka, Japan or PrimeHisto XE, Pacific Image Electronics, New Taipei, Taiwan) at a resolution of 4800 or 5000 pixels per inch. Images from serial sections were aligned on each other using graphics software (Illustrator 10, Adobe, San Jose, CA, USA). Higher magnification images of bright-field specimens were digitized using a cooled color CCD camera (DP-50; Olympus) attached to a microscope (BX41; Olympus). Fluorescence images were digitized using a cooled color CCD camera attached to a fluorescent microscope (BX51WI with DP-70 camera, Olympus or AxioImager. Z2 with AxioCam1Cm1 camera, Zeiss) in 16-bit gray-scale with an appropriate filter set. Using the same exposure parameters, images of all sections processed simultaneously in one immunostaining procedure were taken. Micrographs were adjusted with regard to contrast and brightness and assembled with software (Photoshop 7, Adobe). An appropriate combination of pseudo-color was applied to fluorescent images. Photographs were assembled using Photoshop and Illustrator software. The software was used to adjust contrast and brightness but no other digital enhancements were applied.

Mapping somatosensory responses in the cerebellum

Female Aldoc-Venus mice were anesthetized with ketamine as above. Body temperature was maintained by a heating pad (37°). The mice were fixed in a stereotaxic apparatus (SR-9M, Narishige, Tokyo, Japan) in prone position, 60° nose down. The caudomedial part of the occipital bone was removed and the dura was opened to expose the vermal lobules VII–IX. An epifluorescent image of the exposed cerebellar surface was photographed. A stainless steel wire was placed on the soft tissue near the exposed cerebellum as a reference electrode. Electrical signals were recorded through a glass microelectrode (tip diameter ~ 2 µm) filled with saline via an extracellular monopolar amplifier (MEG-5200, Nihon Kohden, Tokyo, Japan). A bandpass filter (100–10,000 Hz) was used. The signal was monitored via an oscilloscope and an audio device and was digitally recorded by an A-D converter system (micro1401, Cambridge Electronic Design, CED, Milton, Cambridge, UK). Recorded data were analyzed with spike2 software (CED).

Various somatosensory stimulations (brush touch and manual flexion of extremities and tail) were carried out. The recording electrode was placed in the square array positions of 100 µm separation in the midline area and nearby areas of apices of lobule VIII, caudal lobule VII and rostral lobule IX from a depth of 0.3–0.5 mm.

Recording field potential responses to the spinal cord stimulation in the cerebellum

Female mice of B6C3F1 background were anesthetized with medetomidine as above and were fixed in the stereotaxic

apparatus in prone position on a heating pad, with 60° nose down. The sacral spinal cord was exposed as previously described. The membrane covering the dorsal surface of the spinal cord was dissected in the midline. A concentric metal stimulation electrode (USK-10, Unique Medical, Tokyo, Japan) was inserted to a depth of 0.5 mm at the midline.

The caudomedial part of the occipital bone was removed and the dura opened to expose the vermal lobules VII–IX, which was covered by a thin layer of liquid paraffin mixed with mineral oil. A stainless steel wire was placed on the dura with a drop of saline near the exposed cerebellum as a reference electrode. Electrical signals were recorded through a glass microelectrode (tip diameter ~2 µm) filled with saline, monitored, recorded and analyzed as above. Negative pulse stimulation of constant current (0.1 ms duration, 10–30 µA) was given with an interval of about 1 s. Field potential responses were recorded as above from the apparently midsagittal apical position of lobule VIII, which was the center of several positions from which responses to tail flexion were observed before applying electrical stimulation, at the depth of 0.5 mm. The average of 12 responses was obtained by Spike2 software (CED).

Lesioning of lobule VIII and rotarod test

The rotarod test (Sarpong et al. 2018) was performed in Aldoc-Venus mice with lesions of lobule VIII. A pair of littermate female Aldoc-Venus mice (2–3 months old) of similar body weight (a difference of less than 3 g in weight) were tested together. They were anesthetized and secured in a stereotaxic apparatus as above. The occipital bone covering vermal lobules VII, VIII and IX was removed. An epifluorescent image was photographed to identify aldolase C stripes. A hypodermic needle (26G, outer diameter, 0.36 mm) was poked into the center of stripe 1+ in apical lobule VIII, or midline negative stripe (1−) in lobule VII, perpendicular to the surface and down to a depth of 1 mm through the dura, in one of the test pair. No poking was made in the other mouse (sham operation). The skin was sutured and the mice were allowed to recover from the surgery. The rotarod test (below) was performed from the day after the surgery. Ten pairs of mice were tested after lesioning of lobule VIII and another ten pairs, after lesioning of lobule VII. Mice were perfuse-fixed (as above) thereafter and the cerebellum was dissected. Serial coronal or sagittal sections were cut to observe the lesions.

To examine the locomotor performance in Aldoc-Venus mice, we performed the test in a trio of 2- to 3-month-old females of similar body weight (a difference of less than 3 g in weight)—a homozygote, a heterozygote and a wild-type mouse obtained in our colony of Aldoc-Venus mice. Twelve trios were tested.

The rotarod was of a diameter of 30 mm and accelerates linearly from four revolutions per minute (rpm) to 42 rpm in 350 s. During this period, the time until mice dropped from the rod (drop latency) was recorded. The measurements were taken for four successive days, four times daily with an interval of 1 h to obtain the average performance time for the day for each mouse.

Statistical analysis of rotarod test

The daily drop latency of all animals in each group (lobule VIII lesion/sham, lobule VII lesion/sham, and Aldoc-Venus hetero/homo/wild type) was summarized. The average and standard error of the daily drop latency were obtained for each group. The data were also rendered to two-tailed unpaired Student's *t* test using Excel 2016 (Microsoft, Redmond, Washington) to compare the daily drop latency between groups.

Results

Retrograde labeling from lobule VIII

To locate the origin of the spinal projection to the medial longitudinal compartments of lobule VIII, we injected a retrograde tracer into individual zebrin stripes and observed the distribution of retrogradely labeled neurons in the spinal cord, the putative major source of the projection to the midline area of vermal lobule VIII (Matsushita and Ikeda 1980; Reeber et al. 2011; Sengul et al. 2015; Luo et al. 2018). Injections made into stripe 1+ and 1− labeled an abundant cluster of neurons in the sacral segments (Fig. 1a1, 2, b1, 2), but with more sparsely distributed neurons in lumbar, thoracic and cervical segments (75 and 55% of labeled neurons were located in the sacral segments, Table 1). Strongly labeled neurons were distributed in the pericanal gray matter in the sacral segments in these cases (Fig. 1d). Injections into stripe 2+ labeled several neurons in the sacral segments (Fig. 1a3, b3; 21.4% of labeled neurons, Table 1) and a larger number of neurons in other segments. Injections into stripe 2− and stripes in the lateral vermis or paravermis (f− and e1+) labeled a sparse distribution of neurons in the sacral spinal cord (Fig. 1a4–6, b4–6; 3.2–0.5% of labeled neurons, Table 1). These results suggested the presence of a particular population of spinocerebellar projection neurons, from the sacral spinal cord to stripes 1+ and 1− (designated as midline area) in lobule VIII, on which we focused in the succeeding parts of the present study.

To identify the location of the originating cell bodies of this projection within the gray matter of the spinal cord, the distribution of labeled cell bodies was re-mapped on the coronal plane, in cases with injections into stripes 1+

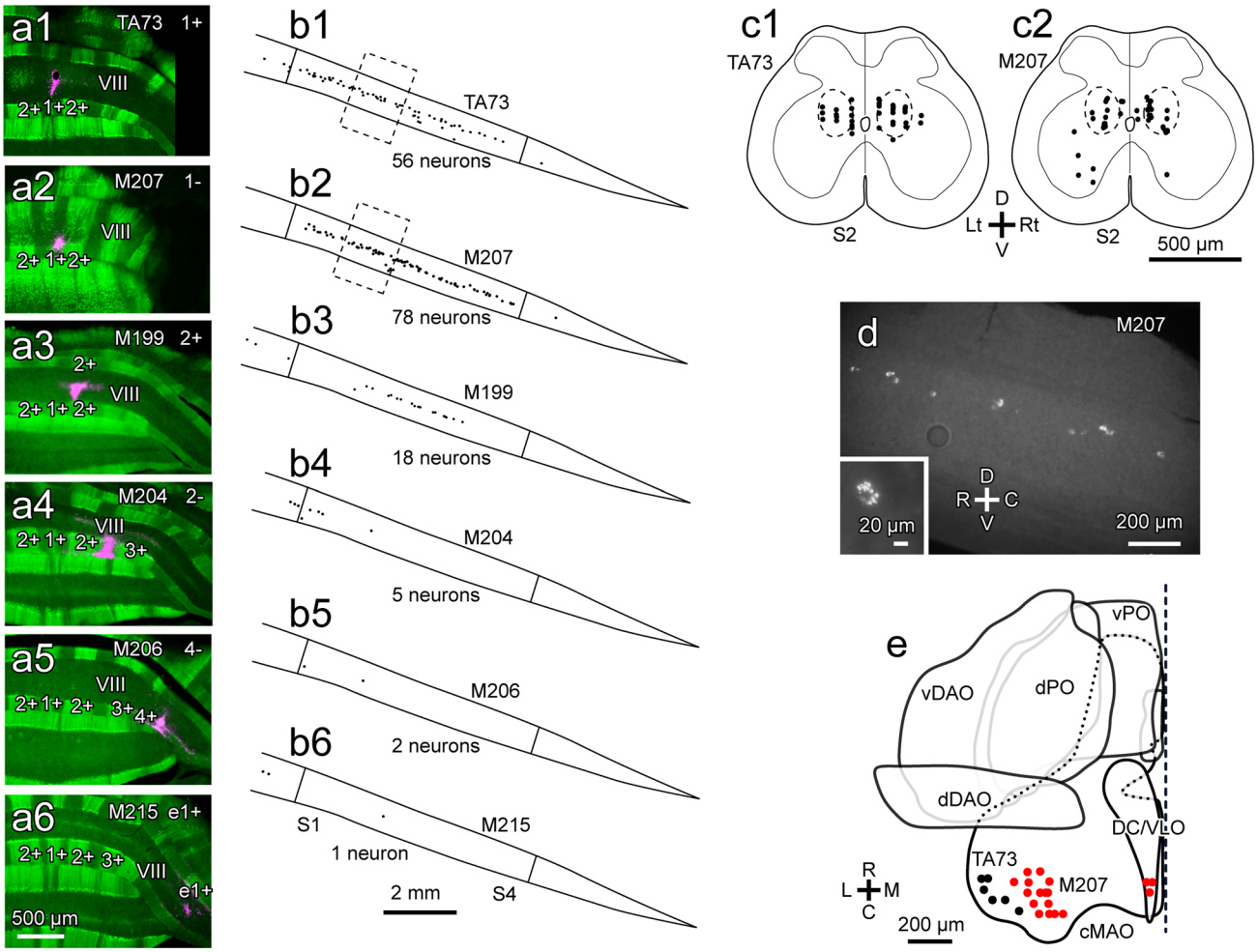

Fig. 1 Retrograde labeling of spinocerebellar neurons in the sacral segments of the spinal cord which project to vermal lobule VIII in the mouse. **a1**–**a6** Digital images of injection sites of the retrograde tracer, fluorescent latex beads (Lumafluor), in zebrin stripes in lobule VIII in six Aldoc-Venus mice. The injection sites were located in stripes 1+, 1−, 2+, 2−, 4− and e1+ from the top to the bottom. **b1**–**b6** Superimposed mapping of retrogradely-labeled neurons in serial sagittal sections in the sacral spinal segments in each mouse. The number of labeled neurons in the sacral segments is indicated. **c1**, **c2** Mapping of retrogradely-labeled neurons in S2 segment onto a coronal plane in two mice (TA73 and M207). Dashed circles indicate the putative location of Stilling's nucleus based on electrophysiological mapping in the rat (Edgley and Grant 1991). **d** Digital images of retrogradely-labeled neurons in a sagittal section at segment S2 in case M207. Inset shows a magnified image of a labeled neuron. **e** Mapping of retrogradely-labeled neurons in the inferior olivary nucleus in two cases (black: injection to stripe 1+, TA73; red: injection to stripe 1−, M207), shown in the horizontal scheme of the left inferior olive (Sarpong et al. 2018). All labeled neurons were located in the caudal part of the medial accessory olive (cMAO). VIII, lobule VIII; C, caudal; D, dorsal; L, lateral; M, medial; R, rostral; S1, S2, S4, sacral segments; V, ventral

Table 1 Distribution of retrogradely labeled neurons in different segments of the spinal cord

Case	TA73	M207	M199	M204	M206	M215
Injection stripe	1+	1−	2+	2−	4−	e1+
Cervical[a]	2	4	7	20	0	1
Thoracic	5	18	12	71	72	90
Lumbar	12	41	47	58	76	124
Sacral	59	78	18	5	2	1
(Percentile)	(74.7%)	(54.9%)	(21.4%)	(3.2%)	(1.3%)	(0.5%)
Coccygeal[a]	1	1	0	0	0	0
Sum	79	142	84	154	150	216

Counted in six cases shown in Fig. 1

[a]The rostral part of the cervical spinal cord and caudal part of the coccygeal spinal cord were not included

and 1− (Fig. 1c). As observed in sagittal sections, most of the labeled neurons were distributed bilaterally in the pericanal gray matter (Fig. 1d) which matched with the location of the Stilling's nucleus (Snyder et al. 1978; Edgley and Grant 1991; dashed circles in Figs. 1c1 and 2). These results indicated that neurons in the Stilling's nucleus were the origin of the spinocerebellar projection to stripes 1+ and 1− in lobule VIII.

These injections also labeled inferior olivary neurons, the origin of climbing fibers. Injections made into stripes 1+ and 1− in lobule VIII labeled neurons in the most caudolateral part and the medially neighboring area (Fig. 1e, black and red, respectively). These areas corresponded to subnuclei a

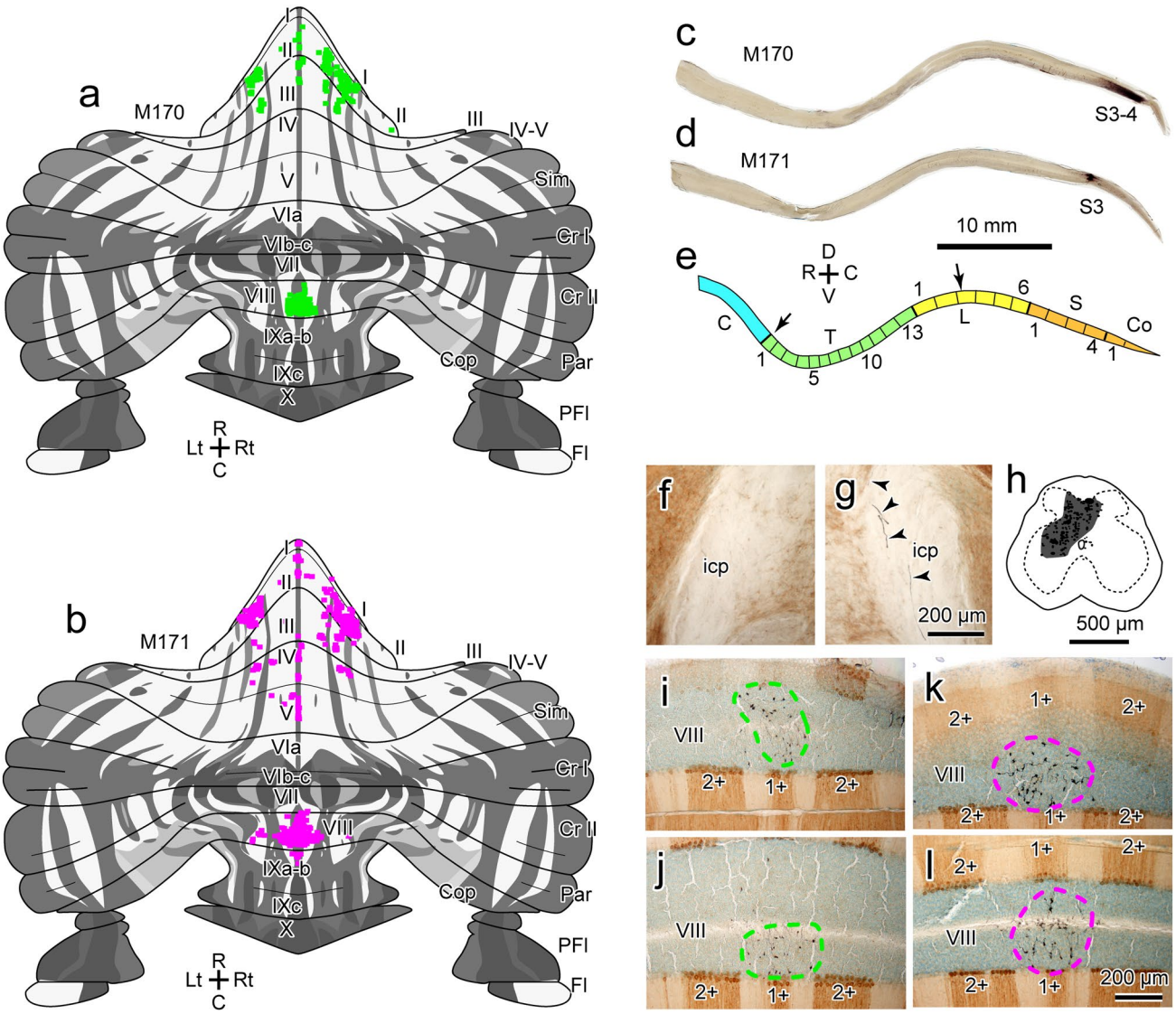

Fig. 2 Distribution of axonal terminals of the spinocerebellar projection originating from the sacral spinal cord in the mouse. **a**, **b** Mapping of all axonal terminals labeled by BDA injection into the sacral spinal cord in two cases (M170 and M171, respectively). Terminals were mapped upon the unfolded scheme of the cerebellar cortex with zebrin (aldolase C) stripes (Sarpong et al. 2018). **c**, **d** Images of the sagittal section of the spinal cord containing the BDA injection site. **e** Scheme of the spinal segmentation (Luo et al. 2018). This scheme was referred to, in order to identify the spinal segment of the injection sites. f and g, Digital image of the left (**f**) and right (**g**) inferior cerebellar peduncle of M171, showing passing axons (arrowheads) only on the right side. **h** Scheme of the coronal trajectory of the reconstructed BDA injection site (shaded area) and labeled somata (black dots) of neurons in the injection site. **i**–**l** Images of coronal sections of the cerebellar cortex (lobule VIII), in which axonal terminals and zebrin stripes were labeled. Dashed lines circumscribe the terminal distribution areas. Panels show sections near the apex (**i**, **k**) and 240 µm deeper areas (**j**, **l**) for M170 (**i**, **j**) and M171 (**k**, **l**). 1+, 2+, stripe 1+, stripe 2+; C, caudal in **a** and **b**, cervical in **e**; Co, coccygeal; Cop, copula pyramidis; Cr I, crus I; Cr II, crus II; D, dorsal; Fl: flocculus; I–X, lobule I–X; icp, inferior cerebellar peduncle; L, lumbar; Lt, left; Par, paramedian lobules; PFl: paraflocculus; R, rostral; Rt, right; S, sacral; Sim, simple lobule; S3–4, S3, sacral segment(s) 3–4 or 3; T, thoracic; V, ventral

and b of the caudal part of the medial accessory olive, which projects to stripes 1+ and 1− respectively, in the rat vermis (Sugihara and Shinoda 2004).

Among the nuclei of mossy fiber sources in the medulla and pons, some neurons in the lateral reticular nucleus (Wu et al. 1999), and basilar pontine nucleus (Biswas et al. 2019) and dorsal column nuclei (Quy et al. 2011; Gebre et al. 2012) project to vermal lobule VIII. To compare the proportion of axonal projections from these sources and the spinal cord to the midline area of lobule VIII, we counted retrogradely labeled neurons in these brain stem nuclei (at both left and right sides), in injections into stripes 1+ and 1−. The basilar pontine nucleus, dorsal column nuclei, and lateral reticular nucleus contained 38, 11 and 34 neurons, respectively (versus 79 neurons in the spinal cord) in the case of the injection into stripe 1+ (case TA73) and 72, 17 and 69 neurons in that same order (versus 142 neurons in the spinal cord) in the case of injection into stripe 1− (case M207). The nucleus X, nucleus prepositus hypoglossi and nucleus reticularis tegmenti pontis also contained a small number (less than 23) of labeled neurons in these cases. The results indicated that, besides spinal cord spinocerebellar neurons a comparable number of neurons in the brain stem also send mossy fibers to the midline area of vermal lobule VIII. However, axons originating from these neurons may have different nuber of terminals in lobule VIII (see "Discussion").

Anterograde axonal tracing from the sacral spinal cord

To clarify the axonal projection pattern of spinocerebellar neurons in the sacral spinal cord, we injected an anterograde tracer, BDA into the left pericanal gray matter of the sacral spinal cord (Fig. 2c–e, h). Although the injection site of the first case (M170) was more caudal relative to that of the second case (M171), the distribution patterns were generally similar between these two cases (Fig. 2c, d). In the anterior lobules, terminals were mainly distributed bilaterally, in stripes 1+ and 2− in lobule II, and sparsely in nearby stripes in vermal lobules II–III. A small number of terminals were distributed bilaterally, in stripes 1+, 1− and 2− in lobules I–V in one case (Fig. 2b). In the posterior lobules, a localized, dense distribution was observed in stripes 1+ and 1−, bilaterally in the apex (Fig. 2i, k) and the caudal wall (Fig. 2j, l) of lobule VIII. A small number of terminals were distributed bilaterally, in stripes 2 + and 2− in lobule VIII, and in stripe 1+ in lobule IX (Fig. 2b). These findings confirmed the projection from the Stilling's nucleus in the sacral spinal cord to stripes 1+ and 1− in lobule VIII (preceding section). Labeled spinocerebellar axons ran in the inferior cerebellar peduncle on the right side (Fig. 2f, g). Neurons labeled by spread of the injected BDA, which were supposed to contain the origin of the labeled spinocerebellar axons, were mostly located on the left side (Fig. 2h). This indicated that labeled axons ascended the pathway contralateral to the location of the soma.

To understand their projection patterns, we reconstructed two individual spinocerebellar axons in one of two cases of BDA injection into the left sacral spinal cord (M170). Two axons were completely traced in the cerebellum and medulla and further down to the cervical spinal cord (Table 2). These axons ascended the dorsal part of the right lateral funiculus and entered the cerebellum through the inferior cerebellar peduncle (Fig. 3a, d) or the "medullary path" as compared to the "pontine path" (Luo et al. 2018). They had no collaterals in the spinal cord or the medulla. After entering the cerebellum, the stem axon gave rise to several branches in the deep cerebellar white matter (Fig. 3b, e). Branches generally ran in the longitudinal direction to enter the lobular white matter and the cortex to further give rise to secondary and more branches which terminated as mossy fibers. This pattern of the axonal path was similar to that of spinocerebellar axons originating from Clarke's column neurons (Luo et al. 2018), except that the pathway of axons in the present study is contralateral to the soma. One of the major branches made a dense terminal arborization with 71 (Axon M170A) and 106 (Axon M170B) mossy fiber terminals in the apex and caudal folial wall of lobule VIII, in midline zebrin-positive stripe 1+ and neighboring zebrin-negative stripe 1−, bilaterally. Other branches terminated in lobules II and III, bilaterally (Fig. 3c) or contralaterally (Fig. 3f), in zebrin stripes 1+, medial 1−, lateral 1−, 2+ and 2−. These axons had no collaterals terminating in the cerebellar nuclei, the medulla or the spinal cord.

The termination pattern of these single axons was similar to the distribution pattern of all terminals of the two cases (M170 and M171, Fig. 2a, b). It suggests that axons with a projection pattern similar to those of axons M170A and M170B were also the main components of labeled terminals in case M171. In sum, the results of the retrograde and anterograde labeling, and single axon reconstruction indicated that neurons in the Stilling's nucleus constitute the major spinocerebellar projection originating from the pericanal gray matter of the sacral spinal cord, and that they make a specific, dense projection to medial stripes (1+ and 1−) in the apex and caudal wall of lobule VIII.

Response to tail flexion

Edgley and Grant (1991) reported that spinocerebellar neurons in Stilling's nucleus respond to passive flexion of the tail in the rat. Therefore, we examined the responsiveness of mossy fiber terminals in zebrin stripes in lobule VIII in

Table 2 Pathway and terminal distribution of two reconstructed spinocerebellar axons labeled by BDA injection into the sacral spinal cord

Axon	Injection site	Axonal pathway			Number of mossy fiber terminals in the cerebellar cortex																Collaterals in the cerebellar nuclei, medulla or spinal cord
		Side in relation to the injection site	Position in the lateral funiculus	Entrance site to the cerebellum	anterior lobules						Posterior lobules						Total number				
					Contralateral paravermis	Contralateral vermis	1+	Ipsilateral vermis	Ipsilateral paravermis	Sum	Contralateral paravermis	Contralateral vermis	1+	Ipsilateral vermis	Ipsilateral paravermis	Sum	Contralateral	Midline	Ipsilateral	Sum	
M170A	S3–4	Contralateral	Dorsal	Medullar	0	57 II, 1−: 7 II, 2+: 6 II, 2−: 39 III, 2−: 5	4 II, 1+: 4	32 II, 1−: 2 II, 2−: 22 III, 2−: 8	0	93 (57%)	0	11 VIII, 1−: 11	54 VIII, 1+: 54	6 VIII, 1−: 6	0	71 (43%)	68	58	38	164	0
M170B	S3–4	Contralateral	Dorsal	Medullar	0	42 II, 1−: 22 II, 2−: 4 II, 3−: 1 III, 1−: 8 III, 2−: 7	10 III, 1+: 10	0	0	52(33%)	0	22 VIII, 1−: 21 VIII, 2+: 1	58 VIII, 1+: 58	26 VIII, 1−: 26	0	106 (67%)	64	68	26	158	0

The two axons shown in this table are the same as illustrated in Fig. 2. The number of mossy fiber terminals is counted separately in zebrin stripes in each lobule

S, sacral; II, III, VIII, lobule II, III, VIII; 1+, 1−, 2+, 2−, zebrin stripe 1+, 1−, 2+, 2−

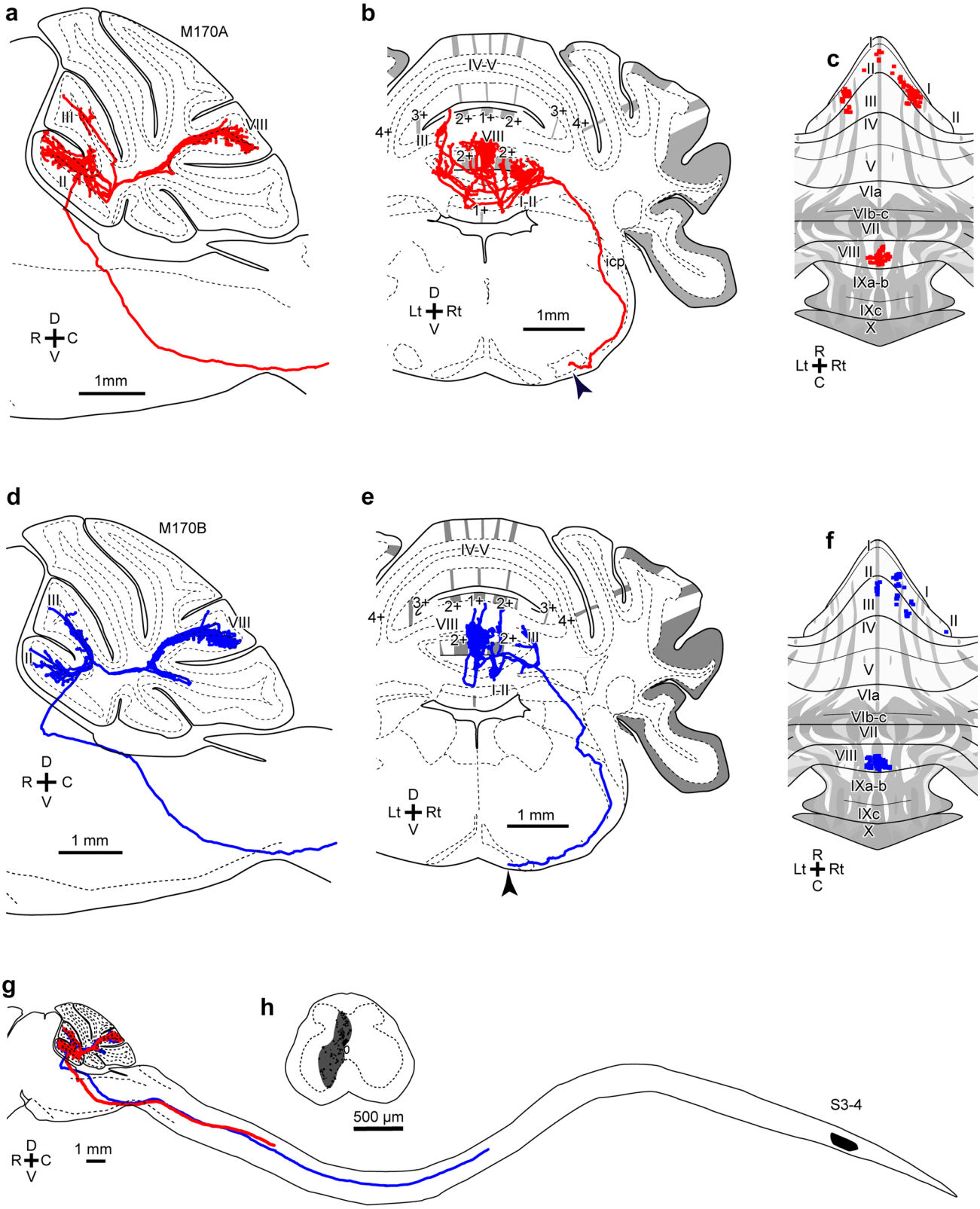

anesthetized Aldoc-Venus mice, in which fluorescence-visualized zebrin stripes facilitated the spatial mapping of responses (Fig. 4f).

Passive flexion of the tail (Fig. 4a, b) resulted in a significant increase in field potential activity recorded at a depth of 0.5 mm in stripe 1+ (Fig. 4c). In expanded traces, positive or

◂**Fig. 3** Reconstruction of two single spinocerebellar axons labeled by BDA injection into the sacral spinal cord (M170A and M170B), axons of putative Stilling's nucleus neurons, in the mouse. Sagittal (**a**) and lateral (**b**) views of the reconstructed axonal trajectory. The axonal trajectory was drawn on a montage of drawings of multiple sections in which major axonal termination or a major axonal path was observed. Arrowheads indicate the trunk of the stem axon in **b**. **c** Mapping of all mossy fiber terminals of this axon upon the unfolded scheme of the cerebellar cortex with zebrin (aldolase C) stripes (Sarpong et al. 2018). **d**–**f** Display of the trajectory and terminal distribution of another axon (M170B) in the same format as in **a**–**c**. **g** Lateral view of the entire axonal trajectory in the brain and spinal cord. H, Reconstruction of the BDA injection site in the coronal section of sacral segment S3. 1+, 2+, 3+, 4+, stripe 1+, 2+, 3+, 4+; C, caudal D, dorsal; I–X, lobule I–X; icp, inferior cerebellar peduncle; Lt, left; R, rostral; Rt, right; S3–4, sacral segments 3–4; V, ventral

positive–negative spike-like events were detected during the period of high activity in response to tail flexion. Some of such spike-like events were superimposable (Fig. 4d) while others were visibly different from each other in wave shape (Fig. 4e). This observation seemed to match with the discrete activity of mossy fiber terminals of multiple axons. The response was evoked most efficiently by the dorsal flexion of the tail. Flexions of the tail in other directions (lateral or ventral flexions) evoked smaller responses. Passive movement of limb joints or cutaneous touch stimulation of various parts of the body was not effective.

We then mapped the positions where passive flexion of the tail (Fig. 4a, b) produced a response activity in the granular layer (depth 0.3–0.5 mm). Nearly all positions in stripes 1+ and 1− showed a response, while other stripes, but for the medial part of stripe 2+ close to 1−, did not (Fig. 4g). Similar results were obtained in three animals (Fig. 4h, contours of different colors). The distribution pattern of the responses matched well with the distribution of mossy fiber terminals of Stilling's nucleus axons (preceding section).

Response to sacral spinal cord stimulation

To further characterize the electrophysiological responses in stripes 1+ and 1− in lobule VIII, we electrically stimulated the gray matter of the sacral spinal cord and analyzed evoked responses from the midline area in lobule VIII. Field potential response was recorded from the apparent midline area, which was identified by mapping the response to tail flexion, in the apex of lobule VIII in the wild-type mouse (Fig. 5). A stimulation with 0.1 ms current pulse of 20–30 μA in the sacral pericanal gray matter produced a positive wave of latency of 4.5 ms and a following negative wave of latency of 6.0 ms. These positive and negative signals were compatible with the mossy fiber volley and excitatory synaptic response at mossy fiber-granule cell synapses (Eccles et al. 1967). This result further confirmed the mossy fiber projection to the midline area of lobule VIII. The conduction velocity estimated from the latency of 4.5 ms was 12 m/s, supposing 55 mm of conduction length of axons in the spinal cord, medulla and cerebellum (Figs. 2c, d, 3g).

Axonal projection pattern of Purkinje cells in stripes 1+ and 1− of lobule VIII

To consider the function of the midline area of lobule VIII, its output circuit was analyzed by labeling Purkinje cell axons with fluorescence-conjugated dextran, injected locally into the molecular and Purkinje cell layers of stripes 1+ or 1− (Fig. 6a, b, insets). Since these injections had little to no spread into the granular layer, labeling of mossy fibers was assumed to be very weak or absent in these experiments. Although climbing fibers may have been labeled by these injections, the terminal arbor of nuclear collaterals of climbing fiber axons is much thinner and has much smaller number of terminals than that of Purkinje cell axons (Sugihara et al. 1999, 2009). Therefore, we concluded that almost all clearly labeled terminals represented Purkinje cell projections. The injection into stripe 1+ labeled terminals in the most medial corner of the rostroventral part of the medial nucleus (Fig. 6a). The injection into stripe 1− labeled terminals in the most medial corner of the caudodorsal part of the medial nucleus (Fig. 6b). Both termination areas are elongated in the rostrocaudal direction with little overlap. We made an injection into stripe 1+ in three mice and another into stripe 1− in two mice (Fig. 6c). Similar distributions of labeled terminals were observed consistently among cases of injections into stripes 1+ and 1− (3 and 2 cases, respectively, Fig. 6d).

The medial nucleus is divided into the caudoventral and rostrodorsal parts which are mainly innervated by Z+ and Z− Purkinje cells, respectively (Sugihara and Shinoda 2007). Purkinje cell axons originating from zebrin stripe 1+, in lobule VIII, innervated the most mediorostral edge of the Z+ part (Fig. 6a, "Z+"), whereas Purkinje cell axons originating from zebrin stripe 1−, in lobule VIII, innervated the most mediocaudal edge of the Z− part (Fig. 6a, "Z−"). Similar projection patterns were observed in other cases of injections as shown in the three-dimensional mapping of the termination areas (Fig. 6c, d). These termination areas occupied the most medial pole of the medial nucleus. The termination area of Purkinje cells in stripe 1+ was located rostroventral to that of Purkinje cells in stripe 1− (Fig. 6d). This positional relationship, rostroventral versus caudodorsal, did not fully fit with the general organization of Z+ and Z− areas into caudoventral and rostrodorsal parts, respectively, in the medial nucleus (Sugihara and Shinoda 2007).

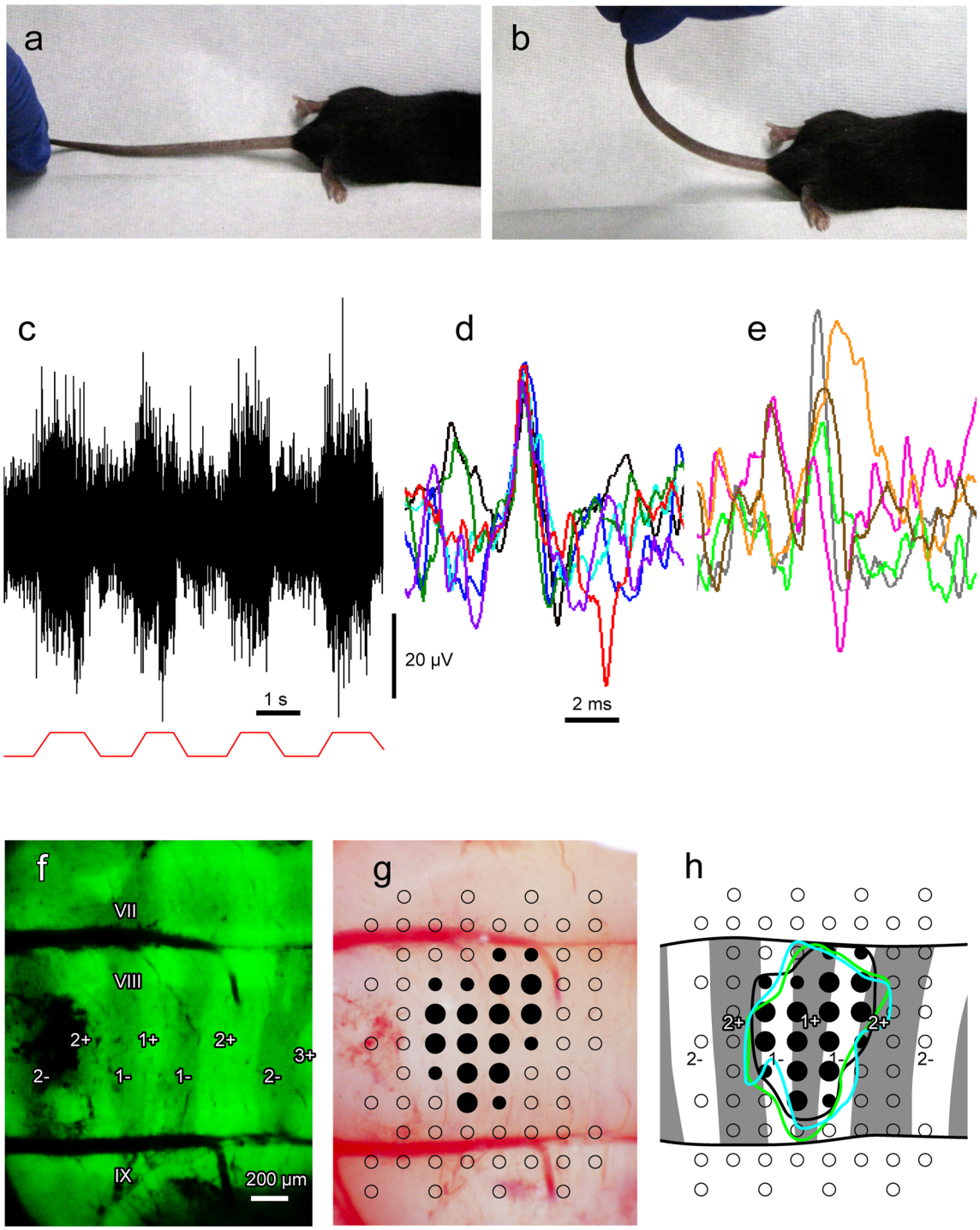

Fig. 4 Electrophysiological mapping of the response to tail flexion in lobule VIII and neighboring lobules. **a**, **b** Images of the dorsal tail flexion which produced the strongest response in the recording area. **c** Signal obtained from the putative granular (0.3 mm deep point in stripe 1+ at the apex of lobule VIII). The attached indented trace approximates the dorsal flexion (and return to the flat position) of the tail. **d**, **e** Signal at the dorsal flexion under high sweep. Six spike-like events of a similar time course (**d**) and five spike-like events of different time courses (**e**) were superimposed. **f** Image of the recording area under epifluorescence. Lobule names and stripe names are indicated. **g** Mapping data were superimposed on the digital image of the same area in a bright field. Open circles, small filled circles, and large filled circles indicate no response, weak response, and strong response, respectively, at a depth of 0.3–0.5 mm. **h** Mapping data were superimposed on the zebrin-striped pattern obtained in the epifluorescence image (**f**). Black curve circumscribes the responsive area in this experiment, while yellow-green and light-blue curves show the responsive area in two other similar experiments aligned on the zebrin stripes

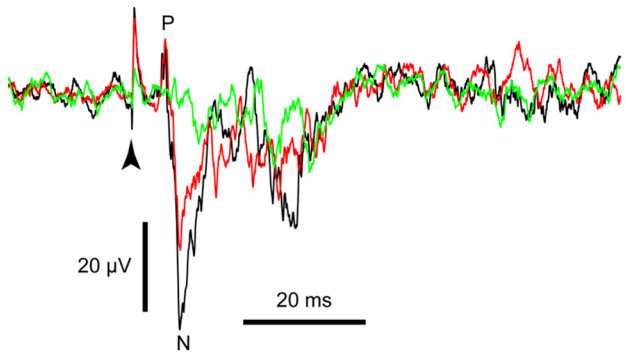

Fig. 5 Evoked potential recorded from the granular layer at the midsagittal apical point in lobule VIII in response to electrical stimulation of the central gray matter of the sacral spinal cord (arrowhead). Average of 12 responses to 10, 20 and 30 μA stimulation are shown (green, red and black, respectively). P and N indicate the initial positive and negative components of the response

Rotarod performance test in mice with a lesion in median lobule VIII

Since the vermal areas of anterior lobules (lobules III–VIa) are involved in the control of locomotion (Muzzu et al. 2018), and that the tail is functionally important for locomotion in rodents (Siegel 1970), there is the possibility that the vermal area of lobule VIII is also involved in the control of locomotion, by utilizing proprioceptive signal from the tail. To examine the involvement of the midline area of lobule VIII in locomotor control, we performed rotarod test in Aldoc-Venus mice in which we made a surgical lesion in stripes 1+ and 1− in lobule VIII by poking with a needle (outer diameter 0.46 mm) to a depth of 1 mm (Fig. 7a). This lesion was intended to damage mossy fiber terminals as well as other components of the cerebellar cortex at the

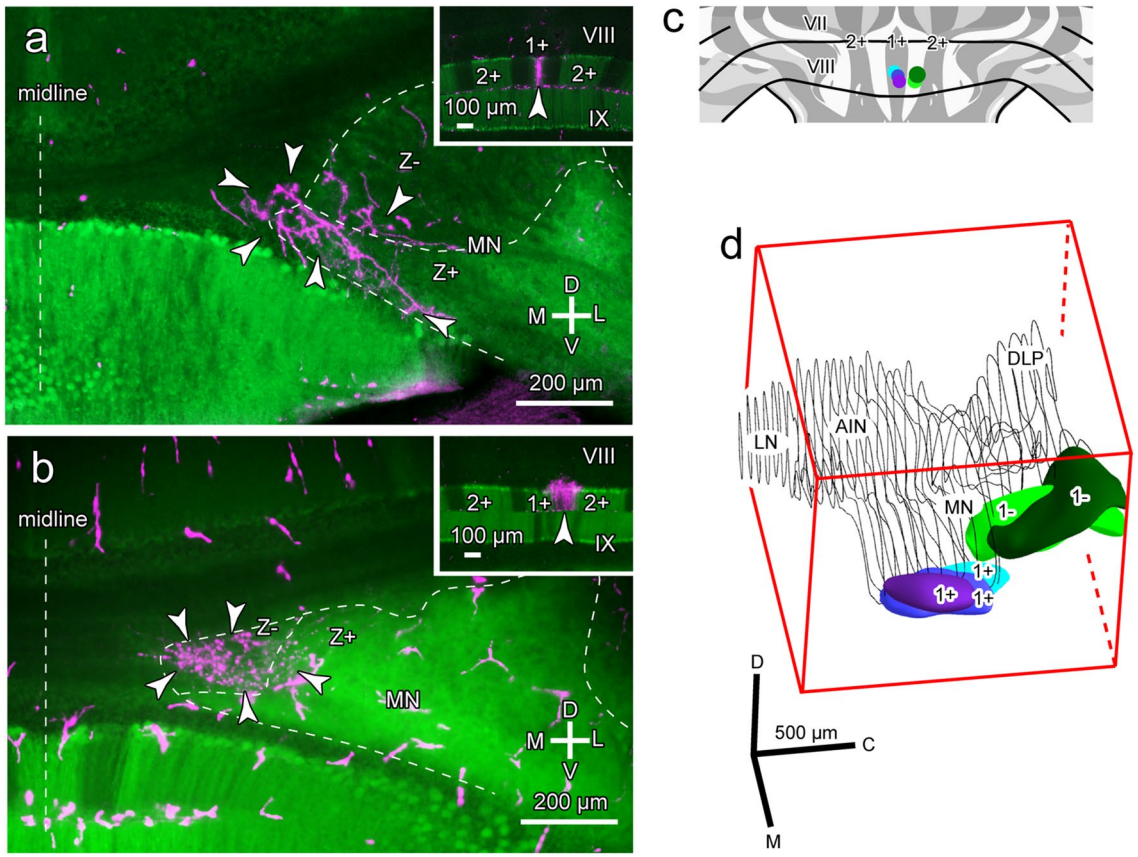

Fig. 6 Purkinje cell projection from zebrin stripes 1+ and 1− in the apex of lobule VIII. **a**, **b** Digital image of axonal termination of Purkinje cells labeled by dextran Alexa Fluor 594 in the cerebellar nuclei. Insets show the injection sites in zebrin stripe 1+ (arrowhead in the inset in **a**) and stripe 1− (arrowhead in the inset in **b**). Arrowheads indicate the labeling of Purkinje cell axons and axonal terminals. Other scattered labelings were presumably produced by nonspecific uptake of the tracer by vascular cells. White dashed lines indicate the midline, contour of the medial nucleus and the boundary between zebrin-positive (Z+) and -negative (Z−) parts of the medial nucleus (Sugihara and Shinoda 2007). **c** Injection sites of five experiments plotted in an unfolded scheme of the cerebellar cortex (Sarpong et al. 2018). **d** Three-dimensional reconstruction of the termination area in the right cerebellar nuclei in a mediodorsal view. Colors in **c** and **d** indicate corresponding cases. The wireframe shows the outline of the cerebellar nuclei in serial coronal sections. AIN, anterior interposed nucleus; C, caudal; D, dorsal; DLP, dorsolateral protuberance of the medial nucleus; L, lateral; LN, lateral nucleus; M, medial; MN, medial nucleus, V, ventral; VII, VIII, IX, lobule VII, VIII, IX

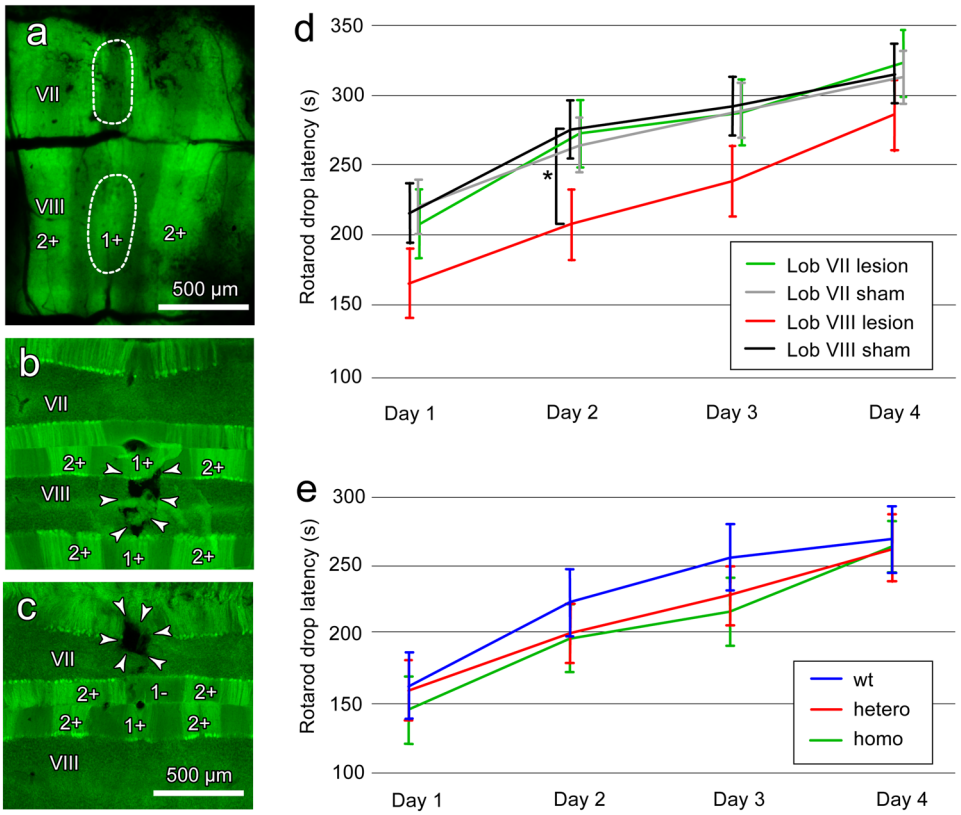

Fig. 7 Rotarod test after lesioning of the midline area of lobules VIII and VII in heterozygous Aldoc-Venus mice. **a** Epifluorescence image of the apexes of lobules VII and VIII on the cerebellar surface of an anesthetized mouse. Lesioning areas were marked with dashed curves in lobules VIII and VII. **b**, **c** Lesioning of lobule VIII (**b**) and VII (**c**) confirmed in coronal sections of the perfuse-fixed brain after the rotarod test. **d** Results of the rotarod test in lesioned mice. **e** Results of the rotarod test in heterozygous, homozygous and wild-type individuals of Aldoc-Venus mice. Single asterisk means $p<0.05$. T [$t_{(11)}$] and P values of unpaired t test were 1.86 and 0.076, 2.12 and 0.046, 1.79 and 0.090, and 1.57 and 0.132 at days 1, 2, 3 and 4, respectively, for lobule VIII lesioning, in **d**. T [$t_{(14)}$] and P values of unpaired t test were 0.23 and 0.813, 0.47 and 0.644, 0.12 and 0.902, and 0.10 and 0.924 at days 1, 2, 3 and 4, respectively, for lobule VII lesioning, in **d**. T [$t_{(12)}$] and P values of unpaired t test were 1.86 and 0.076, 0.83 and 0.412, 0.97 and 0.344, and 0.26 and 0.795 at days 1, 2, 3 and 4, respectively, for wild type/hetero comparison, 0.65 and 0.522, 0.83 and 0.920, 0.41 and 0.684, and 0.08 and 0.93 at days 1, 2, 3 and 4, respectively, for hetero/homo comparison, and 0.87 and 0.395, 1.06 and 0.301, 1.89 and 0.072, and 0.216 and 0.831 at days 1, 2, 3 and 4, respectively, for wild type/homo comparison, in **e**. 1+, 1−, 2+, stipes 1+, 1−, 2+; VII, VIII, lobule VII, VIII

midline apex of lobule VIII (Fig. 7b). Aldoc-Venus mice do not show any apparent phenotypes in locomotor behavior or other behaviors (Fujita et al. 2014). However, we first performed the rotarod test in wild-type, heterozygous and homozygous individuals of Aldoc-Venus strain to further check their baseline locomotor performance. All three groups showed similar learning curves with no significant differences (Fig. 7e). The results indicated a normal locomotor performance of Aldoc-Venus mice in the rotarod test and validated their use in lesioning experiment.

Lesioning of stripes 1+ and 1− in lobule VIII resulted in shorter drop latency with daily improvements (Fig. 7d, red vs. black). The difference was significant on day 2 [$t_{(11)}=2.12$, $p=0.046$, unpaired t test]. Different statistical analyses such as two-way ANOVA with post hoc Tukey test produced similar results. To confirm the lobular specificity of lesion-induced impairment in locomotor performance in another group of mice, we made a similar lesion in the midline area of lobule VII (Fig. 7c), which neighbors lobule VIII but receives mossy fibers not from the spinal cord or the dorsal column nuclei (Quy et al. 2011; Luo et al. 2018) but from other precerebellar nuclei including the pontine nucleus (Biswas et al. 2019). Lesioning of lobule VII did not produce any significant change in locomotor performance (Fig. 7d, green vs. gray). The results suggested that a lesion-induced locomotor impairment is specific to the midline area of lobule VIII.

Discussion

The present results demonstrated a functional localization in the midline area (stripes 1+ and 1−) of lobule VIII in the mouse cerebellar cortex. This area was the specific target

of spinocerebellar axons originating from the Stilling's nucleus, which conveys proprioceptive sensation of the tail. This area innervated the most medial parts of the medial cerebellar nucleus and is possibly involved in the control of locomotion.

Single axon morphology and responsiveness of Stilling's nucleus neurons

Axonal morphology, defined by axonal pathway, branching and termination patterns is one of the essential properties of neurons and provides useful information for classifying neuronal populations. Three groups of spinocerebellar neurons (Clarke's column neurons and two other groups) have been identified based on their axonal morphology, in the thoracic spinal cord (Matsushita and Ikeda 1980; Luo et al. 2018). Stilling's nucleus in the sacral spinal cord, or the sacral precerebellar nucleus, has been regarded as a similar structure to the Clarke's column, or the dorsal nucleus, in the thoracic segments (Snyder et al. 1978; Sengul et al. 2013, 2015). Several aspects of the single axon morphology of Stilling's nucleus neurons, i.e., no collaterals in the spinal cord or the medulla, and bilateral projection to the cerebellum, were similar to those of Clarke's column neurons (Luo et al. 2018). However, the laterality of the ascending path of Stilling's nucleus neurons (contralateral path) did not match with that of the Clarke's column neurons (ipsilateral path), replicating the results of retrograde labeling with spinal cord hemisection (Matsushita and Ikeda 1980).

Edgley and Grant (1991) reported that Stilling's nucleus neurons respond well to passive tail flexion in the horizontal plane in the rat whereas their activity was best responsive to dorsal flexion of the tails in this study. The conduction velocity estimated in the mouse in the present study (12 m/s) was relatively slower than that recorded in the rat (22.8 m/s, Edgley and Grant 1991). The reason for this discrepancy in directional sensitivity or conduction velocity is unclear.

Functional localization in lobule VIII of the cerebellum

While human imaging studies can identify gross active areas in the cerebellum in response to particular behaviors or tasks (Stoodley et al. 2012), animal experiments can demonstrate precisely the functional significance of anatomical compartments defined by lobules and stripes. The three major stripes in the flocculus are involved in the adaptation of reflexive eye movements in different directions (Leonard et al. 1988). Zebrin stripe 5− in the hemispheric lobule VIa near the junction to lobule V, is involved in eyeblink conditioning (Mostofi et al. 2010). Several zebrin stripes in the lateral vermal and paravermal parts of lobules III–V and paravermal parts of lobule VIII have electrophysiologically identified somatosensory climbing fiber inputs (Andersson and Oscarsson 1978; Cerminara et al. 2013).

Locomotion control has been implicated in vermal lobules III–VIa (Muzzu et al. 2018), in which the origins of mossy and climbing fibers are roughly identified (Ji and Hawkes 1994; Gebre et al. 2012). In comparison, an understanding of the functional significance of the vermal posterior lobules (lobule VIII), which may belong to the caudal part of dual somatotopic representation, has been limited. Bilateral lesioning of the lateral vermis of lobules VI, VII and VIII produced no significant deficit in rotarod performance but a disturbance in footprint gait pattern (Stroobants et al. 2013). A study involving selective lesioning and the analysis of climbing fiber input showed that the lateral vermal area of lobule VIII is involved in increasing muscle tone in freezing behavior, but not significantly involved in locomotion (Koutsikou et al. 2014). The most lateral area in the vermal lobule VIII, which is lateral to the above area involved in freezing behavior, has tail representation in climbing fiber response (Atkins and Apps 1997). Input from the Stilling's nucleus has been located relatively widely in lobule VIII and nearby lobules in an electrophysiological study (Edgley and Grant 1991). The present study demonstrated the major mossy fiber projection and granule cell responsiveness to tail proprioception mostly localized in the midline area (stripes 1+ and 1−) of lobule VIII. We, therefore, propose the involvement of this area in locomotion, based on a previous report that the tail is essential in rodent balance and locomotion (Siegel 1970) and on the results of our behavior experiment.

Input–output organization of the midline area of lobule VIII

Among the input and output projections of the cerebellum which contribute to functional localization, the projections of climbing fibers and Purkinje cell axons, and climbing fiber-dependent responses in Purkinje cells are tightly correlated with zebrin stripes (Andersson and Oscarsson 1978; Voogd et al. 2003; Sugihara and Shinoda 2004; Cerminara et al. 2013), a preserved landmark structure of cerebellar compartments (Hawkes and Leclerc 1987).

On the contrary, mossy fiber axonal projections generally show a broad distribution with a significant diversion into multiple zebrin stripes, resulting in an inexplicit link to individual zebrin stripes compared to climbing fiber projections (Wu et al. 1999; Quy et al. 2011; Luo et al. 2018; Biswas et al. 2019). A preserved correlation between mossy fiber projection pattern and a zebrin stripe or subdivision of a zebrin stripe is observed when a mass of mossy fiber axons is labeled (Ji and Hawkes 1994; Reeber et al. 2011; Gebre et al. 2012; Biswas et al. 2019). However, the point-to-point topographical relationship between a single mossy fiber axon from a particular

origin and the target zebrin stripe in a cerebellar lobule has not been clearly described so far. The present study first demonstrated such a precise topographic projection pattern of mossy fiber axons; a population of mossy fiber axons produced a dense cluster of terminals in particular zebrin stripes in a particular lobule in a highly preserved manner among individuals. Whether this type of preserved, precise projection to a particular place occurs in other mossy fiber systems, such as those mapped for facial cutaneous sensation (Welker 1987), would be an interesting observation.

Concerning other mossy fiber inputs, the present study confirmed that the thoracic and lumbar spinal cord (Luo et al. 2018; Reeber et al. 2011), basilar pontine nucleus (Biswas et al. 2019), and lateral reticular nucleus (Wu et al. 1999) send a substantial number of axons to the midline area of vermal lobule VIII. However, our previous anterograde labeling and axonal reconstruction studies have shown that their axons do not make a dense terminal arbor at their target position, but rather terminate with a small number of branches and sparse terminals in the midline area of vermal lobule VIII (Biswas et al. 2019; Luo et al. 2018; Wu et al. 1999). Therefore, the projection from the Stilling's nucleus, which produces axons with a dense terminal arbor, seems to be the sole predominant input to the midline area (zebrin stripes 1+ and 1−) of vermal lobule VIII. Besides, the present study suggested a weak projection from the dorsal column nuclei (Quy et al. 2011; Gebre et al. 2012), nucleus X, nucleus prepositus hypoglossi and nucleus reticularis tegmenti pontis to the midline area of vermal lobule VIII.

Concerning the output projection, neighboring areas of stripes 1+ and 1− of lobule VIII project to two areas in the most medial part of the medial nucleus. Each of these two areas was situated at the most medial edge of one of the two major divisions (ventrocaudal and rostrodorsal parts) of the cerebellar nuclei defined by the projections of zebrin-positive and -negative Purkinje cells (Sugihara and Shinoda 2007). These areas are included within and/or overlapped with the area where electrical stimulation evoked locomotion (Mori et al. 1998), and c-fos activity was detected after a locomotion task (Ruigrok et al. 1996). Their output neurons project mainly to the vestibular nuclei, medullar and pontine reticular formation (Teune et al. 2000), which are descending motor control centers. These findings support the idea that the output pathway of the midline area in lobule VIII may be involved in the control of locomotion. The impairment of motor activity after lesioning of this area supports this idea. It is a question as to whether the two most medial areas in the medial nucleus project to different targets of the cerebellum or are involved in distinct functions. Another unresolved question is how the convergence of Purkinje cell projections from lobule VIII and anterior lobules (lobules I–VIa) occur in these nuclear areas.

Climbing fiber input to the midline area of vermal lobule VIII should have a significant contribution to its function. The results showed that the caudolateral pole of the medial accessory olive is the origin of climbing fiber projections to stripes 1+ and 1− in lobule VIII. The results matched with findings in a rat study (Sugihara and Shinoda 2004). Anatomical studies have shown that the lateral part of the medial accessory olive receives innervation from the lower lumbar and sacral spinal cord (Boesten and Voogd 1975; Matsushita et al. 1992) and expresses c-Fos after a locomotion task (Ruigrok et al. 1996). Whether this part of the inferior olive receives somatosensory signals from the tail would be an interesting observation. The suitable stimulation that evokes climbing fiber activity in stripes 1+ and 1− in lobule VIII needs to be clarified.

The origins of climbing fiber input to stripe 1+ and 1− were proximate but distinct in the inferior olive (Fig. 1). The targets of PCs in these stripes were also proximate but distinct in the cerebellar nuclei. This relationship may suggest similar but slightly different functions between these stripes, as shown in pairs of zebrin-positive and -negative stripes in lobules IXcd–X of the pigeon cerebellum (Long et al. 2018).

Possible mechanisms of information integration in the midline area of lobule VIII

A focal lesioning of the midline area in lobule VIII produced a detectable impairment of locomotor behavior. This finding suggests that the proprioceptive information conveyed by the Stilling's nucleus projection is utilized in information processing for locomotion. It is a question as to how such integration occurs in this area. The granule cells that are innervated by these axons send parallel fibers to wide areas in lobule VIII, not only to stripes 1+ and 1−. Synapses in the ascending part of granule cells may have a stronger effect on Purkinje cells in the same stripe (Gundappa-Sulur et al. 1999). The granule cell signal is either excitatory when directly conveyed through parallel fiber-Purkinje cell synapses or inhibitory when conveyed through interneurons to Purkinje cells. The effectiveness of these synapses may be modulated by climbing fiber-dependent or other mechanisms. Another synaptic effect can be the inhibition by Golgi cells, which make dense axonal terminals and zebrin-arranged spread of dense dendritic arbor (Sillitoe et al. 2008). Thus, Golgi cell function may be correlated with the clustered mossy fiber terminals of the Stilling's nucleus projection.

With the dense cluster of mossy fiber terminals of a known origin localized directly underneath, stripes 1+ and 1− in lobule VIII seem to be suitable positions to examine information processing in the cerebellar cortex. The modulation of simple spike activity in Purkinje cells in different

zebrin stripes by tail flexion or by Stilling's nucleus stimulation may be a possible experiment.

Acknowledgements This study was supported by Grant-in-Aid for Scientific Research from the Japan Society for the Promotion of Science (16K07025 to I. S., 18H06085 to Y. L.). The authors thank Dr. Gideon Sarpong and Mr. Richard Nana Abankwah Owusu Mensah for proofreading the manuscript and Mr. Viet T. Nguyen-Minh for comments on statistical analyses.

Author contributions Conceptualization: YL, TO, IS; methodology: YL, TO, IS; Formal analysis and investigation: YL, TO, XW, KS, IS; writing and funding acquisition: YL and IS; resources: KS, IS; supervision: IS.

Compliance with ethical standards

Conflict of interest The authors have no conflict of interest to declare.

Ethical approval This study involved no human participants but animals. Experimental protocols were approved by the Animal Care and Use Committee (A2018-147C, A2018-260C, A2018-222C, A2017-063A, A2017-062A, 017097A) and Gene Recombination Experiment Safety Committee (2012-064C4, 2017-040A) of Tokyo Medical and Dental University. This study was supported by Grant-in-Aid for Scientific Research from the Japan Society for the Promotion of Science (16K07025 to I. S., 18H06085 to Y. L.).

References

Andersson G, Oscarsson O (1978) Climbing fiber microzones in cerebellar vermis and their projection to different groups of cells in the lateral vestibular nucleus. Exp Brain Res 32:565–579. https://doi.org/10.1007/BF00239553

Atkins MJ, Apps R (1997) Somatotopical organisation within the climbing fibre projection to the paramedian lobule and copula pyramidis of the rat cerebellum. J Comp Neurol 389:249–263. https://doi.org/10.1002/(SICI)1096-9861(19971215)389:2%3c249:AID-CNE5%3e3.0.CO;2-1

Biswas MS, Luo Y, Sarpong GA, Sugihara I (2019) Divergent projections of single pontocerebellar axons to multiple cerebellar lobules in the mouse. J Comp Neurol 527:1966–1985. https://doi.org/10.1002/cne.24662

Boesten AJ, Voogd J (1975) Projections of the dorsal column nuclei and the spinal cord on the inferior olive in the cat. J Comp Neurol 161:215–237. https://doi.org/10.1002/cne.901610206

Brochu G, Maler L, Hawkes R (1990) Zebrin II: a polypeptide antigen expressed selectively by Purkinje cells reveals compartments in rat and fish cerebellum. J Comp Neurol 291:538–552. https://doi.org/10.1002/cne.902910405

Cerminara N, Aoki H, Loft M, Sugihara I, Apps R (2013) Structural basis of cerebellar microcircuits in the rat. J Neurosci 33:16427–16442. https://doi.org/10.1523/JNEUROSCI.0861-13.2013

Eccles JC, Sasaki K, Strata P (1967) Interpretation of the potential fields generated in the cerebellar cortex by a mossy fibre volley. Exp Brain Res 3:58–80. https://doi.org/10.1007/BF00234470

Edgley SA, Grant GM (1991) Inputs to spinocerebellar tract neurons located in Stilling's nucleus in the sacral segments of the rat spinal cord. J Comp Neurol 305:130–138. https://doi.org/10.1002/cne.903050112

Ekerot CF, Oscarsson O, Schouenborg J (1987) Stimulation of cat cutaneous nociceptive C fibres causing tonic and synchronous activity in climbing fibres. J Physiol 386:539–546. https://doi.org/10.1113/jphysiol.1987.sp016550

Fujita H, Aoki H, Ajioka I, Yamazaki M, Abe M, Oh-Nishi A, Sakimura K, Sugihara I (2014) Detailed expression pattern of aldolase C (Aldoc) in the cerebellum, retina and other areas of the CNS studied in Aldoc-Venus knock-in mice. PLoS ONE 9:e86679. https://doi.org/10.1371/journal.pone.0086679

Gebre SA, Reeber SL, Sillitoe RV (2012) Parasagittal compartmentation of cerebellar mossy fibers as revealed by the patterned expression of vesicular glutamate transporters VGLUT1 and VGLUT2. Brain Struct Funct 217:165–180. https://doi.org/10.1007/s00429-011-0339-4

Gundappa-Sulur G, De Schutter E, Bower JM (1999) Ascending granule cell axon: an important component of cerebellar cortical circuitry. J Comp Neurol 408:580–596. https://doi.org/10.1002/(SICI)1096-9861(19990614)408:4%3c580:AID-CNE11%3e3.0.CO;2-O

Harrison M, O'Brien A, Adams L, Cowin G, Ruitenberg MJ, Sengul G, Watson C (2013) Vertebral landmarks for the identification of spinal cord segments in the mouse. Neuroimage 68:22–29. https://doi.org/10.1016/j.neuroimage.2012.11.048

Hawkes R, Leclerc N (1987) Antigenic map of the rat cerebellar cortex: the distribution of parasagittal bands as revealed by monoclonal anti-Purkinje cell antibody mobA113. J Comp Neurol 256:29–41. https://doi.org/10.1002/cne.902560104

Horn KM, Pong M, Gibson AR (2010) Functional relations of cerebellar modules of the cat. J Neurosci 30:9411–9423. https://doi.org/10.1523/JNEUROSCI.0440-10.2010

Ji Z, Hawkes R (1994) Topography of Purkinje cell compartments and mossy fiber terminal fields in lobules II and III of the rat cerebellar cortex: spinocerebellar and cuneocerebellar projections. Neuroscience 61:935–954. https://doi.org/10.1016/0306-4522(94)90414-6

Koutsikou S, Crook JJ, Earl EV, Leith JL, Watson TC, Lumb BM, Apps R (2014) Neural substrates underlying fear-evoked freezing: the periaqueductal grey-cerebellar link. J Physiol 592:2197–2213. https://doi.org/10.1113/jphysiol.2013.268714

Larsell O (1952) The morphogenesis and adult pattern of the lobules and fissures of the cerebellum of the white rat. J Comp Neurol 97:281–356. https://doi.org/10.1002/cne.900970204

Leonard CS, Simpson JI, Graf W (1988) Spatial organization of visual messages of the rabbit's cerebellar flocculus. I. Topology of inferior olive neurons of the dorsal cap of Kooy. J Neurophysiol 60:2073–2090. https://doi.org/10.1152/jn.1988.60.6.2073

Long RM, Pakan JMP, Graham DJ, Hurd PL, Gutierrez-Ibañez C, Wylie DR (2018) Modulation of complex spike activity differs between zebrin-positive and -negative Purkinje cells in the pigeon cerebellum. J Neurophysiol 120:250–262. https://doi.org/10.1152/jn.00797.2017

Luo Y, Patel RP, Sarpong GA, Sasamura K, Sugihara I (2018) Single axonal morphology and termination to cerebellar aldolase C stripes characterize distinct spinocerebellar projection systems originating from the thoracic spinal cord in the mouse. J Comp Neurol 526:681–706. https://doi.org/10.1002/cne.24360

Matsushita M, Ikeda M (1980) Spinocerebellar projections to the vermis of the posterior lobule and the paramedian lobule in the cat, as studied by retrograde transport of horseradish peroxidase. J Comp Neurol 192:143–162. https://doi.org/10.1002/cne.901920110

Matsushita M, Yaginuma H, Tanami T (1992) Somatotopic termination of the spino-olivary fibers in the cat, studied with the wheat germ agglutinin-horseradish peroxidase technique. Exp Brain Res 89:397–407. https://doi.org/10.1007/BF00228255

Mori S, Matsui T, Kuze B, Asanome M, Nakajima K, Matsuyama K (1998) Cerebellar-induced locomotion: reticulospinal control of spinal rhythm generating mechanism in cats. Ann N Y Acad Sci 860:94–105. https://doi.org/10.1111/j.1749-6632.1998.tb09041.x

Mostofi A, Holtzman T, Grout AS, Yeo CH, Edgley SA (2010) Electrophysiological localization of eyeblink-related microzones in rabbit cerebellar cortex. J Neurosci 30:8920–8934. https://doi.org/10.1523/JNEUROSCI.6117-09.2010

Muzzu T, Mitolo S, Gava GP, Schultz SR (2018) Encoding of locomotion kinematics in the mouse cerebellum. PLoS ONE 13:e0203900. https://doi.org/10.1371/journal.pone.0203900

Nguyen-Minh VT, Tran-Anh K, Luo Y, Sugihara I (2019) Electrophysiological excitability and parallel fiber synaptic properties of zebrin-positive and -negative Purkinje cells in lobule VIII of the mouse cerebellar slice. Front Cell Neurosci 12:513. https://doi.org/10.3389/fncel.2018.00513

Pijpers A, Apps R, Pardoe J, Voogd J, Ruigrok TJ (2006) Precise spatial relationships between mossy fibers and climbing fibers in rat cerebellar cortical zones. J Neurosci 26(46):12067–12080. https://doi.org/10.1523/JNEUROSCI.2905-06.2006

Quy PN, Fujita H, Sakamoto Y, Na J, Sugihara I (2011) Projection patterns of single mossy fiber axons originating from the dorsal column nuclei mapped on the compartments in the rat cerebellar cortex. J Comp Neurol 519:874–899. https://doi.org/10.1002/cne.22555

Reeber SL, Gebre SA, Sillitoe RV (2011) Fluorescence mapping of afferent topography in three dimensions. Brain Struct Funct 216:159–169. https://doi.org/10.1007/s00429-011-0304-2

Ruigrok TJH (2011) Ins and outs of cerebellar modules. Cerebellum 10:464–474. https://doi.org/10.1007/s12311-010-0164-y

Ruigrok TJH, van der Burg H, Sabel-Goedknegt E (1996) Locomotion coincides with c-Fos expression in related areas of inferior olive and cerebellar nuclei in the rat. Neurosci Lett 214:119–122. https://doi.org/10.1016/0304-3940(96)12898-6

Sarpong GA, Vibulyaseck S, Luo Y, Biswas MS, Fujita H, Hirano S, Sugihara I (2018) Cerebellar modules in the olivo-cortico-nuclear loop demarcated by pcdh10 expression in the adult mouse. J Comp Neurol 526:2406–2427. https://doi.org/10.1002/cne.24499

Sengul G, Watson C, Tanaka I, Paxinos G (2013) Atlas of the spinal cord: of the rat, mouse, marmoset, rhesus, and human. Academic Press, Amsterdam

Sengul G, Fu Y, Yu Y, Paxinos G (2015) Spinal cord projections to the cerebellum in the mouse. Brain Struct Funct 220:2997–3009. https://doi.org/10.1007/s00429-014-0840-7

Siegel MI (1970) The tail, locomotion and balance in mice. Am J Phys Anthropol 33:101–102. https://doi.org/10.1002/ajpa.1330330113

Sillitoe RV, Chung SH, Fritschy JM, Hoy M, Hawkes R (2008) Golgi cell dendrites are restricted by Purkinje cell stripe boundaries in the adult mouse cerebellar cortex. J Neurosci 28:2820–2826. https://doi.org/10.1523/JNEUROSCI.4145-07.2008

Snyder RL, Faull RL, Mehler WR (1978) A comparative study of the neurons of origin of the spinocerebellar afferents in the rat, cat and squirrel monkey based on the retrograde transport of horseradish peroxidase. J Comp Neurol 181:833–852. https://doi.org/10.1002/cne.901810409

Stoodley CJ, Valera EM, Schmahmann JD (2012) Functional topography of the cerebellum for motor and cognitive tasks: an fMRI study. Neuroimage 59:1560–1570. https://doi.org/10.1016/j.neuroimage.2011.08.065

Stroobants S, Gantois I, Pooters T, D'Hooge R (2013) Increased gait variability in mice with small cerebellar cortex lesions and normal rotarod performance. Behav Brain Res 241:32–37. https://doi.org/10.1016/j.bbr.2012.11.034

Sugihara I, Shinoda Y (2004) Molecular, topographic and functional organization of the cerebellar cortex: a study with combined aldolase C and olivocerebellar labeling. J Neurosci 24:8771–8785. https://doi.org/10.1523/JNEUROSCI

Sugihara I, Shinoda Y (2007) Molecular, topographic, and functional organization of the cerebellar nuclei: analysis by three-dimensional mapping of the olivonuclear projection and aldolase C labeling. J Neurosci 27:9696–9710. https://doi.org/10.1523/JNEUROSCI

Sugihara I, Wu H, Shinoda Y (1999) Morphology of single olivocerebellar axons labeled with biotinylated dextran amine in the rat. J Comp Neurol 414:131–148. https://doi.org/10.1002/(SICI)1096-9861(19991115)414:2%3c131:AID-CNE1%3e3.0.CO;2-F

Sugihara I, Fujita H, Na J, Quy PN, Li BY, Ikeda D (2009) Projection of reconstructed single Purkinje cell axons in relation to the cortical and nuclear aldolase C compartments of the rat cerebellum. J Comp Neurol 512:282–304. https://doi.org/10.1002/cne.21889

Teune TM, Burg JV, Moer JV, Voogd J, Ruigrok T (2000) Topography of cerebellar nuclear projections to the brain stem in the rat. Prog Brain Res 124:141–172. https://doi.org/10.1016/S0079-6123(00)24014-4

Voogd J, Ruigrok TJH (1997) Transverse and longitudinal patterns in the mammalian cerebellum. Prog Brain Res 114:21–37. https://doi.org/10.1016/S0079-6123(08)63356-7

Voogd J, Pardoe J, Ruigrok TJH, Apps R (2003) The distribution of climbing and mossy fiber collateral branches from the copula pyramidis and the paramedian lobule: congruence of climbing fiber cortical zones and the pattern of zebrin banding within the rat cerebellum. J Neurosci 23:4645–4656. https://doi.org/10.1523/JNEUROSCI.23-11-04645.2003

Welker W (1987) Spatial organization of somatosensory projections to granule cell cerebellar cortex: functional and connectional implications of fractured somatotopy (summary of Wisconsin studies). In: King JS (ed) New concepts in cerebellar neurobiology. Alan R.Liss, New York, pp 239–280

Wu H, Sugihara I, Shinoda Y (1999) Projection patterns of single mossy fibers originating from the lateral reticular nucleus in the rat cerebellar cortex and nuclei. J Comp Neurol 411:97–118. https://doi.org/10.1002/(SICI)1096-9861(19990816)411:1%3c97:AID-CNE8%3e3.0.CO;2-O